THE JOURNAL OF PHYSICAL CHEMISTRY B

Article

Cite This: J. Phys. Chem. B 2018, 122, 4149−4158

pubs.acs.org/JPCB

Star Block-Copolymers in Shear Flow

Diego Jaramillo-Cano,[†] Maud Formanek,[†,§] Christos N. Likos,*[,†] and Manuel Camargo*[,‡]

[†]Faculty of Physics, University of Vienna, Boltzmanngasse 5, A-1090 Vienna, Austria

[‡]Centro de Investigaciones en Ciencias Básicas y Aplicadas, Universidad Antonio Nariño, Km 18 via Cali-Jamundí, 760030 Cali, Colombia

ABSTRACT: Star block-copolymers (SBCs) have been demonstrated to constitute self-assembling building blocks with specific softness, functionalization, shape, and flexibility. In this work, we study the behavior of an isolated SBC under a shear flow by means of particle-based multiscale simulations. We systematically analyze the conformational properties of low-functionality stars, as well as the formation of attractive patches on their corona as a function of the shear rate. We cover a wide range of system parameters, including functionality, amphiphilicity, and solvent quality. It is shown that SBCs display a richer structural and dynamical behavior than athermal star polymers in a shear flow [Ripoll et al. *Phys. Rev. Lett.*, **2006**, *96*, 188302], and, therefore, they are also interesting candidates to tune the viscoelastic properties of complex fluids. We identify three factors of patch reorganization under shear that lead to patch numbers and orientations depending on the shear rate, namely, free arms joining existing patches, fusion of medium-sized patches into bigger ones, and fission of large patches into two smaller ones under high shear rates. Because the conformation of single SBC is expected to be preserved in low-density bulk phases, the presented results are a first step in understanding and predicting the rheological properties of semidilute suspensions of this kind of polymers.

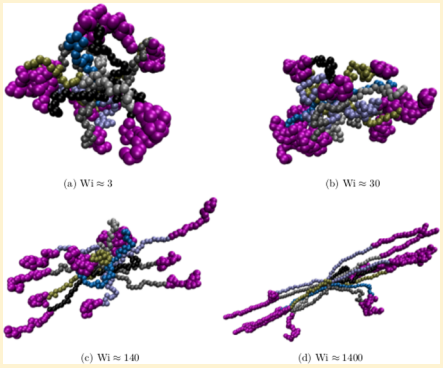

INTRODUCTION

In the recent years, theoretical and computational research about the specific design of microscopic building blocks able to self-assemble into desired ordered or disordered macroscopic phases has gained great interest. Remarkable examples of such systems are patchy particles consisting of colloidal particles decorated with distinct functionalized spots (patches) on their surfaces, which give rise to anisotropic and highly directional interactions with other particles. Depending on the number of patches, their location on the colloidal surface, temperature, and particle concentration, a broad spectrum of self-assembly processes can be realized.[2−5] A soft and flexible version of these particles based on star block-copolymers (SBCs) has been proposed recently.[6−8] These star-shaped macromolecules consist of f linear polymer chains (arms) of N_{pol} monomers each, with one of their ends anchored to a central core. Moreover, each arm is an amphiphilic AB diblock-copolymer with an athermal, solvophilic inner segment (A-type monomers), followed by thermosensitive, solvophobic monomers (B-type) at the outermost segment.

Because SBCs can display both intramolecular and intermolecular association phenomena, a great deal of work has been devoted to the study of their conformational features in equilibrium, as well as the structure of their suspensions.[6,7,9−12] These studies have established that isolated SBCs behave as self-associating patchy particles, i.e., they self-assemble into structures with one or multiple aggregation sites or clusters of their solvophobic segments, whose number and extent can be tuned by different factors such as functionality (f), temperature, solvent quality, and/or the fraction of solvophobic monomers. Furthermore, when several aggregation sites are present, these are distributed equally over the whole solid angle due to entropic effects and therefore SBCs resemble soft penetrable colloids with attractive patches, such patchiness being a robust property of the SBCs throughout a broad range of polymer concentrations.[6]

The understanding of the role that conformation and softness of polymer-based assemblies have on the rheological properties of their suspensions, on the other hand, is of considerable interest from both fundamental and applied perspectives.[13,14] Extensive simulation studies have considered the behavior of isolated polymers of diverse architectures (linear, ring, starlike, and hyperbranched) in shear flow, demonstrating particular features due to the conformational degrees of freedom, which distinguish them sharply from rigid colloidal particles.[1,15−21] In the particular case of athermal star polymers, i.e., stars without solvophobic end groups, it has been shown that their structural flexibility leads to a mutual influence of fluid and polymer, resulting in both a change in the conformation of the star and a deviation from the mean velocity profile of the fluid. In addition, stars with small functionality f exhibit a tumbling motion characterized by alternating collapsed and stretched conformations, resembling the behavior of linear polymers, whereas high-functionality stars perform a

Received: December 12, 2017
Revised: March 7, 2018
Published: March 16, 2018

DOI: 10.1021/acs.jpcb.7b12229
J. Phys. Chem. B 2018, 122, 4149−4158

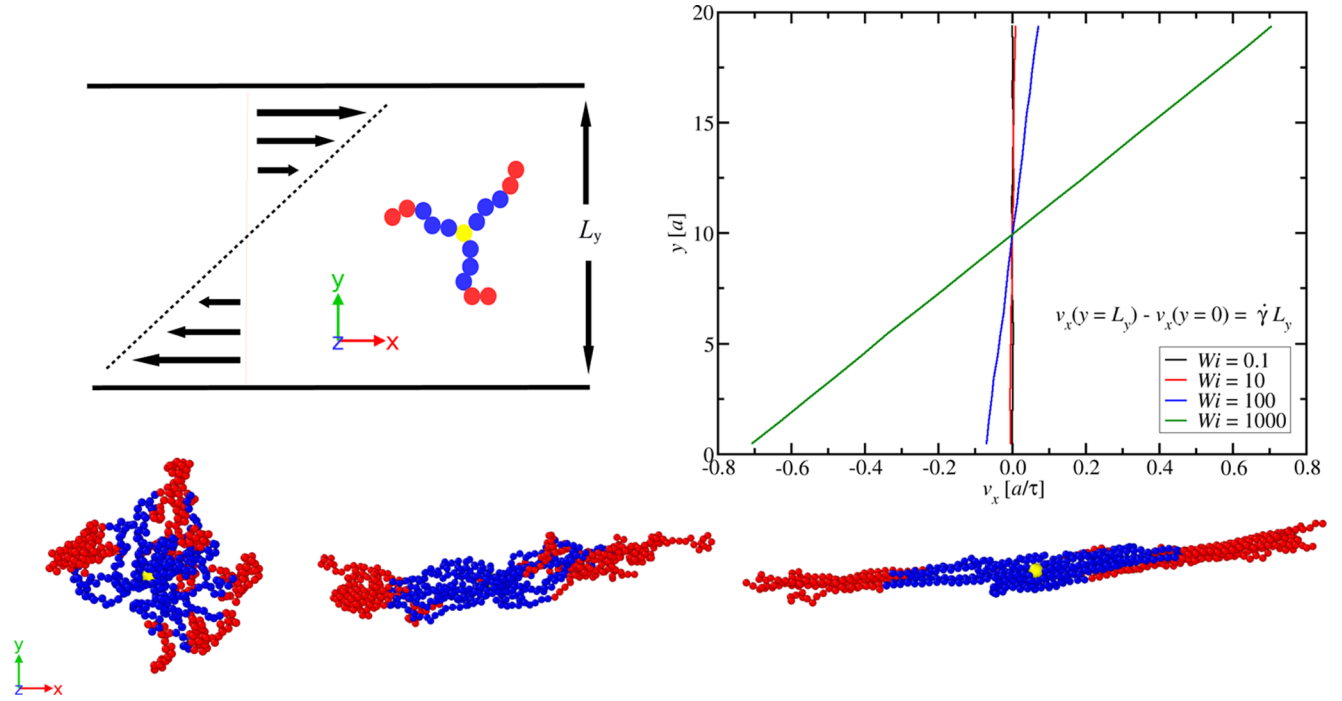

Figure 1. Top left: Schematic illustration of the simulation setup, demonstrating the shear (x), gradient (y), and vorticity (z) directions of planar, Couette flow. Top right: velocity profiles for the pure solvent obtained in our MPCD simulation for different shear rates $\dot{\gamma}$, corresponding to the Weissenberg numbers Wi of the polymer that are indicated in the legend. We emphasize that no polymer was dissolved in this case and the Wi is only used as a convenient way to characterize the flow strength. Bottom: representative conformations of a SBC, viewed from the vorticity axis and projected on the xy-plane (flow-gradient plane). Here, $f = 15$, $\alpha = 0.3$, and $\lambda = 1.1$. Snapshots are shown at equilibrium (left), intermediate ($Wi \simeq 50$, middle), and high shear rates ($Wi \simeq 10^3$, right). Yellow, red, and blue spheres correspond respectively to the star core, solvophobic (B type) monomers, and solvophilic (A type) monomers.

continuous tank-treading rotation similar to fluid droplets and capsules.[1,19] Furthermore, telechelic, stiff linear polymers assemble in equilibrium into scaffold-like networks, whose properties are governed by polymer flexibility and end-attraction strength. Shear flow induces significant structural changes featuring three major rheological regimes, depending on the strength of the applied shear flow.[22,23]

In this work, we investigate the structural properties of isolated, moderate-functionality ($12 \leq f \leq 18$) SBCs under the influence of homogeneous, linear shear flow by means of a hybrid simulation approach, which combines standard molecular dynamics (MD) for the monomers and multiparticle collision dynamics (MPCD) for the solvent particles.[24,25] We quantitatively analyze the behavior of the shape and patchiness of a SBC at several amphiphilicities and solvent qualities using $Wi = \dot{\gamma}\tau_Z$ as a measure of the shear rate $\dot{\gamma}$. As detailed below, the shear rate is expressed in terms of a common, equilibrium Zimm-relaxation time τ_Z of a purely repulsive (athermal) chain with polymerization degree N_{pol}. We span a range of Weissenberg numbers Wi from zero (equilibrium) to the order of 10^3, the latter lying into the nonlinear regime, as schematically represented in Figure 1.

The rest of the paper is organized as follows: in the next section, we briefly present the model and the simulation technique. Afterward, we show and discuss our findings for the geometric features, i.e., sizes and shapes, of SBCs under shear. Particular attention is subsequently being paid to the question of patch reorganization as a consequence of shear, and finally we summarize and draw our conclusions.

METHODS

Star Polymer Model. We simulate a single SBC immersed in a Newtonian solvent by means of a hybrid MPCD-MD method. The star polymers are modeled in the way introduced in ref 7. Each arm of the SBC is represented by means of a bead-spring model with N_A inner and N_B outer monomers ($N_{pol} = N_A + N_B$), therefore, defining the amphiphilicity of the star as $\alpha = N_B/N_{pol}$. In this work, we consider $N_{pol} = 40$ and $\alpha = 0.3$, 0.5, and 0.7. We emphasize that the arm length is thereby much shorter than the one used in ref 7 because the much longer chains used there would require much bigger simulation boxes to be used for the high shear rates, in which the molecules stretch dramatically. As a consequence, the patchiness in equilibrium differs from that found in ref 7, although the general trends are similar in both cases.

The monomers are represented as soft spheres of diameter σ and mass M interacting through pair potentials $V_{AA}(r) = V_{AB}(r) = V(r; 0)$ and $V_{BB}(r) = V(r; \lambda)$, where

$$V(r;\lambda) = \begin{cases} V_0(r) + (1-\lambda)\epsilon & r \leq r_c \\ \lambda V_0(r) & r > r_c \end{cases} \quad (1)$$

Here, $V_0(r) = 4\epsilon[(\sigma/r)^{48} - (\sigma/r)^{24}]$, $r_c = 2^{1/24}\sigma$, and λ is an attraction-controlling coupling constant, which allows us to modulate the solvent quality for the B-monomers; as explained in ref 7, to take $\lambda > 0.92$ is equivalent to considering that a polymer made of B-monomers is below its θ-temperature. We consider ϵ and σ as units of energy and length, respectively, whereas the unit of mass is set by the mass m of the MPCD-solvent particles to be specified below. The bonding between

DOI: 10.1021/acs.jpcb.7b12229
J. Phys. Chem. B 2018, 122, 4149−4158

connected monomers is introduced by a finitely extensible nonlinear elastic potential

$$U_{\mathrm{bond}}(r) = -\frac{1}{2}K\,R_0^2\,\ln\left[1-\left(\frac{r}{R_0}\right)^2\right] \tag{2}$$

where $K = 30(\epsilon/\sigma^2)$ and $R_0 = 1.5\,\sigma$.

Simulation Technique. Multiparticle collision dynamics[24,25] (MPCD) was employed to mesoscopically simulate the solvent. The latter is assumed to be composed of N_s pointlike particles of mass m, whose dynamics follow two steps: a streaming step, in which the solvent particles move ballistically, and a collision step, in which the solvent particles exchange linear momentum. To do that, the particles are sorted into cubic cells with length a and their relative velocities with respect to the center of mass of the cell are rotated by an angle χ around a random axis.[1,24,25] The number of solvent particles per MPCD collision cell is $\rho = 5$ and their mass is $m = M/\rho$, serving as the unit of mass of the simulation; accordingly, the unit of time is defined as $\tau = \sqrt{m\sigma^2/\epsilon}$. For the temperature T, we choose the value $k_BT/\epsilon = 0.5$, where k_B is the Boltzmann constant. The remaining MPCD parameters were set as follows: the time between collisions is $\Delta t_{\mathrm{mpcd}} = 0.1\,\tau$, the rotation angle is $\chi = 130°$, and the cell size $a = \sigma$, making the presence of two monomer centers in the collision cell very unlikely. The Lees–Edwards boundary conditions were used to generate a shear velocity field $\mathbf{v}(y) = \dot{\gamma}y\hat{\mathbf{x}}$, which is characterized by the shear rate $\dot{\gamma}$. To ensure the correctness of the MPCD implementation, static and dynamic properties of the pure solvent were tested. For example, by averaging the x-velocity of the center of mass of each cell, the velocity profile $v_x(y)$ was determined for the range of shear rates employed afterward to probe the star polymer, as shown in the top-right panel of Figure 1.

In the MD section of the hybrid technique, the time evolution of the monomers follows the Newtonian equations of motion, which are integrated with the help of the Velocity-Verlet scheme[26] using an integration time step $\Delta t_{\mathrm{md}} = 10^{-3}\,\tau$. The coupling between the monomers of the SBC and the solvent particles is achieved during the collision step, in which the former are included as point particles in the evaluation of the center-of-mass velocity of each cell and their velocities are also randomly rotated. It is important to note that this interaction is strong enough to keep the monomers at the desired temperature, once a thermostat for the solvent particles has been introduced, which in the present case corresponds to a cell-level Maxwell–Boltzmann scaling.[27] To obtain a dimensionless measure of the shear rate, we consider the Weissenberg number Wi, which is the product of the shear rate with the longest relaxation time of the polymer. For the latter, we take the longest Zimm relaxation time τ_Z of a polymer with N_{pol} monomers, which is given by the expression[1,28]

$$\tau_Z = \frac{\eta_s}{k_BT}\sigma^3 N_{\mathrm{pol}}^{3\nu} \tag{3}$$

where η_s is the (MPCD) solvent viscosity and $\nu = 3/5$ is the Flory exponent for self-avoiding chains. We obtain $\tau_Z \simeq 1.3 \times 10^4\,\tau$ for the specific choices of the MPCD collision parameters and the value $N_{\mathrm{pol}} = 40$ employed here. Although we neglect any dependence of the relaxation time on star functionality and attraction strength along the arms, the results justify a posteriori the choice of a common relaxation time, in the sense that we are able to obtain results for the shape parameters that mostly collapse on one another when plotted against $Wi = \dot{\gamma}\tau_Z$.

We performed 14 independent runs with different initial conditions for each set of parameters $\{f, \alpha, \lambda, Wi\}$ investigated. A preparation run of 5×10^6 MD steps was executed in first place, which was long enough for the SBC to reach its stationary state and then a production cycle of 1.5×10^7 MD steps took place. Depending on the shear rate, the simulation box has dimensions $60\,\sigma \le L_x \le 110\,\sigma$ and $L_y = L_z = 60\,\sigma$. Data for shape parameters, patch number, and patch sizes were evaluated every 2×10^4 MD steps and averaged during the production cycle.

RESULTS AND DISCUSSION

Sizes and Shapes. The overall conformation of the star polymers under different shear rates was analyzed using shape parameters that are defined by means of the invariants of the gyration tensor $\mathbf{G}$. The components of the latter are given by

$$G_{\mu\nu} = \frac{1}{N_{\mathrm{mon}}}\sum_{i=1}^{N_{\mathrm{mon}}}(r_{i,\mu} - r_{\mathrm{cm},\mu})(r_{i,\nu} - r_{\mathrm{cm},\nu}) \tag{4}$$

where $r_{i,\mu}$ and $r_{\mathrm{cm},\mu}$ are the μ components ($\mu = 1$, 2, and 3) of the positions of the ith monomer and of the center of mass of the star, respectively. The considered shape parameters are the asphericity δ, the prolateness S, and the acylindricity c, defined as

$$\delta = 1 - 3\left\langle \frac{I_2}{I_1^2} \right\rangle \tag{5}$$

$$S = \left\langle \frac{1}{I_1^3}\prod_{\mu=1}^{3}(3\lambda_\mu - I_1) \right\rangle \tag{6}$$

$$c = \left\langle \frac{\lambda_2 - \lambda_3}{I_1} \right\rangle \tag{7}$$

In the above equations, λ_k ($k = 1$, 2, 3) indicates the eigenvalues of $\mathbf{G}$, ordered as $\lambda_1 \ge \lambda_2 \ge \lambda_3$, whereas $I_1 = \lambda_1 + \lambda_2 + \lambda_3$ and $I_2 = \lambda_1\lambda_2 + \lambda_2\lambda_3 + \lambda_3\lambda_1$. Note that the radius of gyration of the SBC is given by $R_{\mathrm{gyr}}^2 = I_1$. The first shape parameter, δ, is positive definite and quantifies the asphericity; the second one $-0.25 \le S \le 2$ indicates prolateness ($S > 0$) or oblateness ($S < 0$), and the last parameter $c \ge 0$ quantifies the cylindrical symmetry of the star, with $c = 0$ indicating a perfect cylindrical conformation.[7]

The global conformational features of the SCB at different shear rates are summarized in Figures 2 and 3. In first place, the dependency on Wi of the radius of gyration (R_{gyr}) and of both the asphericity (δ) and the acylindricity (c) parameters are reported in Figure 2. In general, SBCs feature a smaller spatial extension R_{gyr} than their athermal counterparts, the difference between the two growing for larger values of α and λ. The radius of gyration of all the systems increases with shear rate, a feature attributed to the stronger stretching along the flow direction, which overcompensates for the concomitant shrinking in the gradient and vorticity directions. Referring in particular to the inset of the upper panel of Figure 2, we can distinguish, roughly, three regions in the dependence of the polymer size on Wi. For $Wi \lesssim 10$, the macromolecules essentially maintain their equilibrium sizes and conformations, whereas for $10 \lesssim Wi \lesssim 400$, shear has a profound influence on

DOI: 10.1021/acs.jpcb.7b12229
J. Phys. Chem. B 2018, 122, 4149–4158

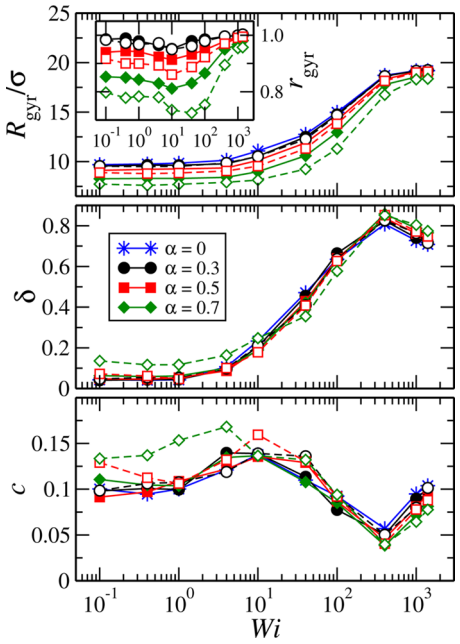

Figure 2. Average shape descriptors as a function of the Weissenberg number for f = 15 and polymerization degree N_{pol} = 40. Radius of gyration (top), asphericity (middle), and acylindricity (bottom) are shown for λ = 1.0 (filled symbols and continuous lines) and λ = 1.1 (empty symbols and dashed lines). Blue stars indicate the data for pure repulsive stars (λ = 0 or α = 0). Inset: normalized radius of gyration $r_{gyr} = R_{gyr}/R_{gyr}^{(ath)}$, where $R_{gyr}^{(ath)}$ is the corresponding value for athermal stars at a given Wi.

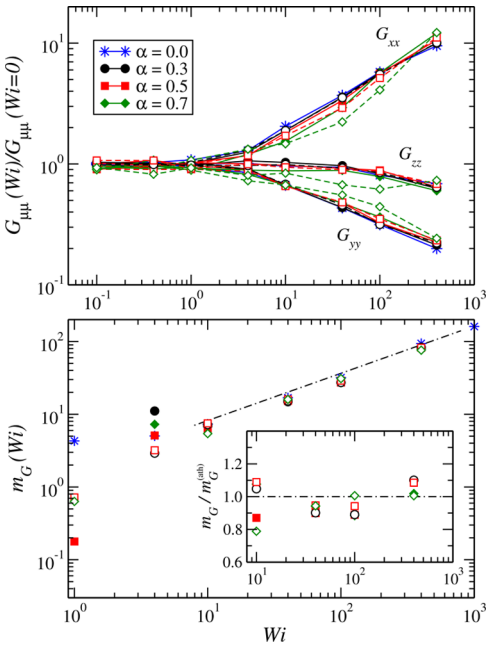

Figure 3. Diagonal components of the gyration tensor (top panel) and orientational resistance (bottom panel) at different shear rates for f = 18, λ = 1.0 (filled symbols and continuous lines) and λ = 1.1 (empty symbols and dashed lines). In the inset, data for m_G are normalized by a factor $m_G^{(ath)} = 0.84\, f^{0.27}\, Wi^{0.65}$, which corresponds to the scaling law (dash−dot lines) found for athermal stars at $Wi \gtrsim 10$.[1]

the shape and conformation of the stars, leading to rearrangements of the attractive patches and changes in their number and orientation, as will be shown in more detail in what follows.

In this regime, the ratio r_{gyr} of the gyration radius of the SBCs to that of the athermal stars has a nonmonotonic dependence on Wi, as shown in the inset of the upper panel of Figure 2, a manifestation of the strong rearrangements of the SBC arms. Finally, in the very strong shear regime, Wi > 400, the arms of the SBCs become strongly stretched and all stars tend to very similar, elongated conformations. In particular, the arms of all SBCs are forced to stretch and the gyration radius of all molecules approaches the same value as that of athermal stars. On the other hand, the behavior of the asphericity δ suggests that as the shear rate increases, the SBC loses its spherical symmetry and develops a rodlike shape ($\delta \to 1$), whose associated acylindricity drops monotonically for 10 < Wi < 400. As before, δ and c tend to the same values of the athermal stars for high Wi, it being particularly notorious for the case α = 0.7 and λ = 1.1, which displays a clearly different global shape with respect to the other SBCs for Wi < 10.

An interesting feature in Figure 2 is a "kink" in the asphericity and in the acylindricity at the highest values of the Weissenberg number (Wi > 400), which is also found for the vorticity-component G_{zz} of the gyration tensor. This kink is caused by a combination of shear-induced confinement of the stars, the strong steric interactions, and crowding at the star core, as well as the relatively short arm length, N_{pol} = 40. Characteristic snapshots that help visualize the conformation of the SBCs under shear are shown at the bottom panels of Figure 1, as well as in Figure 4. At low values of Wi, the stars are hardly distorted, whereas for $Wi \gtrsim 10$, the molecules become increasingly anisotropic, expanding in the flow direction and shrinking most strongly in the shear direction and less so along the vorticity axis. Around the value $Wi \simeq 400$, the confinement in the gradient direction is so strong that the stars resemble two-dimensional objects.[29] Beyond this point, no further shrinkage along the vorticity direction is possible any more because the arms become strongly stretched and the steric hindrance close to the anchoring point in the center pushes these stretched, rodlike arms back out into the vorticity direction. In the employed model of the SBC, the anchoring points of arms to core are allowed to freely glide along the core surface, i.e., the grafting points are not spatially fixed. As a consequence, for Wi > 400, an antagonistic effect appears between the shear-induced shrinkage and the strong monomer packing close to the core poles; as mentioned above, the crowding at the poles becomes so strong that the arms start getting ejected sideways along the vorticity direction (see the bottom panels of Figure 4). This behavior is associated with the kink of shape−descriptors curves at a very high Wi. Because it does not reflect the general features of the SCB, we consider it no further. At this point, it is also worth noting that, at high Wi, loose arms rotate in the flow-vorticity plane in the course of the SBC's tank-treading-like motion, getting reattached to the extended arms at the two ends of the star, whereas other ones leave those patches to perform further rotations. The rich dynamics of the SBC motion in shear fields is, however, a topic that bears detailed analysis on its own, and it will be the subject of future work.

The above considerations on the shape of the stars are quantified by the analysis of the diagonal components $G_{\mu\mu}(Wi)$ ($\mu = x, y, z$) of the gyration tensor as a function of Wi, shown in Figure 3. There is a remarkable collapse of almost all curves for the reduced quantities (over their value at equilibrium, Wi = 0), irrespective of the α- or λ-values; an exception is the extreme case f = 18, α = 0.7, λ = 1.1, which forms three "bulky" patches

DOI: 10.1021/acs.jpcb.7b12229
J. Phys. Chem. B 2018, 122, 4149−4158

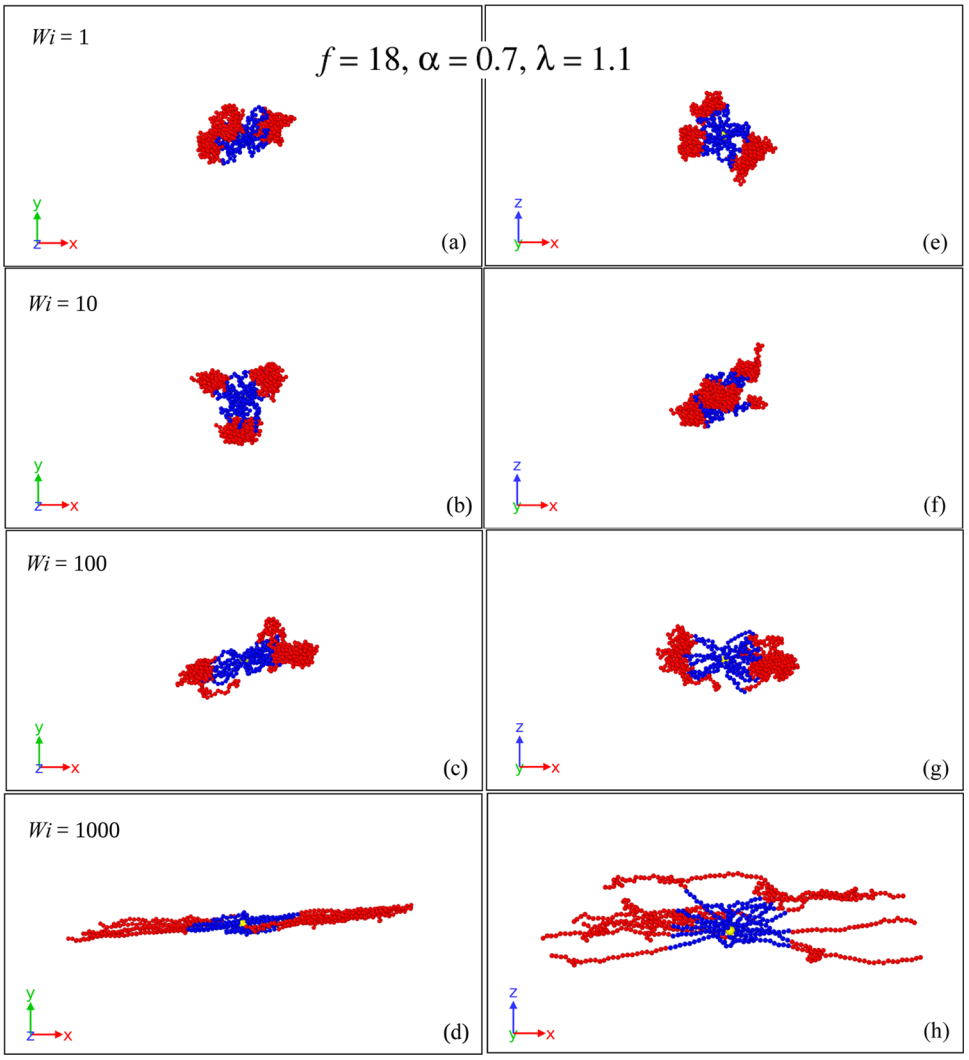

Figure 4. Typical simulation snapshots[30] of the SBC with parameters $f = 18$, $\alpha = 0.7$, and $\lambda = 1.1$ under shear at the Wi values indicated on the legends. Panels (a)−(d) show the view from the vorticity axis on the flow-gradient plane at the given Weissenberg numbers, whereas for panels (e)−(h), the same snapshot as at the panel on the left is shown from the gradient axis looking onto the vorticity-flow plane. The solvophilic monomers are rendered as blue beads and solvophobic ones as red beads.

at equilibrium and thus does not deform under shear as strongly as the other molecules do. As a further global parameter to characterize the conformation of the SBC, we consider the orientational resistance m_G, which measures the average alignment of the polymer induced by the flow and is related to the angle χ_G formed between the eigenvector $\hat{\mathbf{e}}_1$ associated with the largest eigenvalue λ_1 and the flow ($\hat{\mathbf{x}}$) direction. This is defined in terms of the components of the gyration tensor as[1]

$$\frac{m_G}{Wi} = \tan(2\chi_G) = \frac{2G_{xy}}{G_{xx} - G_{yy}} \tag{8}$$

The bottom panel of Figure 3 displays the orientational resistance of the SBCs, demonstrating a remarkable insensitivity to the details of the molecular architecture for a fixed functionality f. Neither the strength of the attraction nor the fraction of attractive monomers affects the orientational resistance, which in fact follows, for sufficiently high values of Wi, the same power law as athermal stars, $m_G^{(ath)} \propto f^{0.27}Wi^{0.65}$. Though the individual values of the diagonal and the flow-gradient components of the gyration tensor differ among different SBCs, these differences cancel out once the ratio of eq 8 is formed and the orientational resistance becomes a universal quantity.

Shear-Induced Patch Reorganization. After grasping the characteristics of the global conformation of the stars, we now focus our attention on the features of the patches, i.e., the clusters formed by the solvophobic monomers of the outer block. In the limit $\lambda \to 0$, no patches are formed in equilibrium. The same is observed for low amphiphilicities ($0 < \alpha < 0.3$) and the values of λ considered here ($0.9 \le \lambda \le 1.1$).[6,10] In such cases, the entropic intrastar repulsions dominate over the enthalpic attractions between the solvophobic tails and the stars behave in the same manner as athermal stars.[31] For $\alpha \ge 0.3$, patches form, whose number N_p and population S_p first increase as the attraction coupling constant λ does, whereas subsequently N_p decreases again as different patches start merging into bigger ones.[7] Because both athermal and amphiphilic star polymers elongate and take on a more prolate shape under linear shear conditions,[1,20] it is to be expected that applying shear on SBC promotes clustering and leads to an

DOI: 10.1021/acs.jpcb.7b12229
J. Phys. Chem. B 2018, 122, 4149−4158

increase in patch number and size compared to equilibrium conditions.

To characterize the behavior of the formed patches under shear, we evaluate the distribution $P(N_p)$ of the number of clusters found per SBC, its average value $\langle N_p \rangle$ and the corresponding distribution $P(S_p)$, and the average $\langle S_p \rangle$ for the patch population (size); the latter represents the number of arms bonded together in a given patch ($S_p \geq 2$). Patches are defined by a threshold-based clustering algorithm in the same way as in ref 7, where two arms are defined to belong to the same cluster if at least two of their B-monomers (one in each arm) are connected neighbors, i.e., their distance is less than the threshold value of $r_{cluster} = 1.1\ \sigma$. The quantity

$$F = f - \langle N_p \rangle \langle S_p \rangle \tag{9}$$

is also introduced to express the typical number of free arms present (i.e., not belonging to any patch) in the configuration. We discuss the three generic types of behavior emerging from our numerical experiments and the underlying mechanisms of patch organization and rearrangements in what follows. In Figure 5, we display the dependence of $P(N_p)$ on different

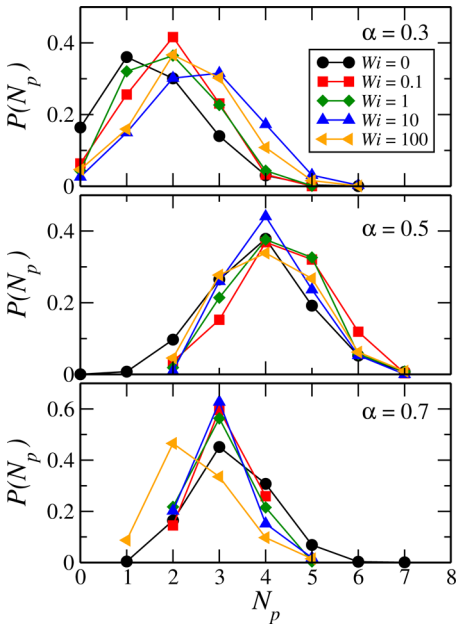

Figure 5. Distribution of the number of patches for $f = 18$ and $\lambda = 1.1$. Note the different scales in vertical axis.

shear rates for the case $f = 18$ and $\lambda = 1.1$ with three different values of the fraction of attractive monomers: $\alpha = 0.3$, 0.5, and 0.7. The behavior shown there is characteristic of all the cases studied and then summarized in Figure 6 for the expectation value $\langle N_p \rangle$, so that a discussion of its features covers all the cases studied. At the same time, the information on the number of patches should be read in conjunction with the distribution $P(S_p)$ of the number of arms participating in the patch and the expectation value $\langle S_p \rangle$, shown in Figures 7 and 8, respectively.

Let us start with the smallest fraction of attractive monomers, $\alpha = 0.3$. In this case, many arms are unattached to any patch at equilibrium and there is even a finite probability that there exist zero patches, i.e., all the arms are unattached, see Figure 5, top panel. For such an initial situation, the shear fields bring about an increasing trend of both the number of patches N_p and the number of arms participating in the patch, S_p. Indeed, the

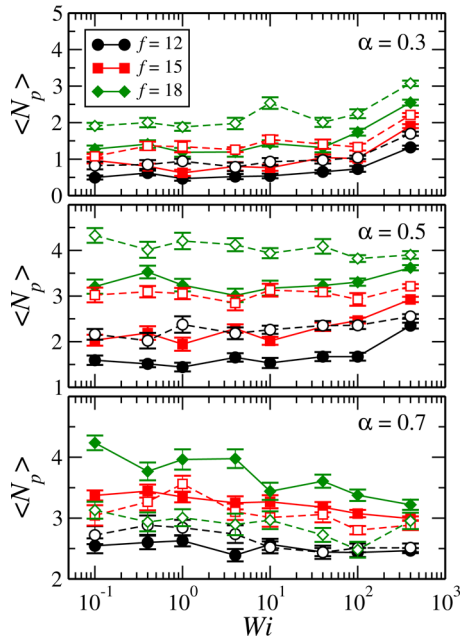

Figure 6. Average number of patches as a function of the Weissenberg number for SBC of different functionality ($N_{pol} = 40$) at $\lambda = 1.0$ (filled symbols and continuous lines) and $\lambda = 1.1$ (empty symbols and dashed lines).

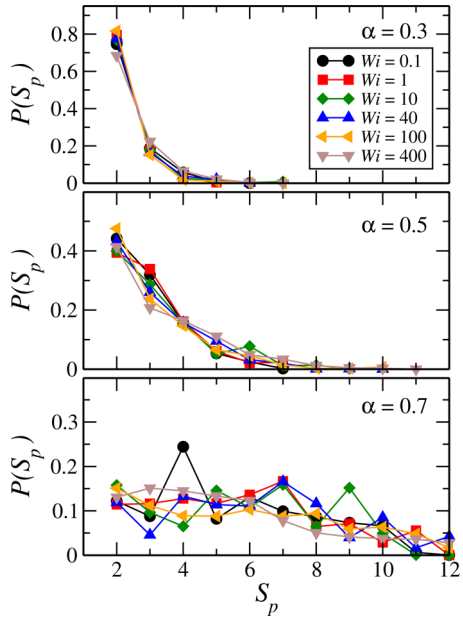

Figure 7. Distribution of patch population for $f = 18$, polymerization degree $N_{pol} = 40$, $\lambda = 1.1$. Note the different scales in vertical axis.

distribution $P(N_p)$ of Figure 5 moves to the right and the probability of finding no patches becomes strongly suppressed; similarly, the expectation value $\langle N_p \rangle$ slowly grows with *Wi*, as can be seen in the top panel of Figure 6. The growth of the number of patches is accompanied by a growth also of the patch population, see Figure 8. It follows that the effect of the shear for such SBCs for which many arms are free at equilibrium ($F \gg 1$) is to bring nonassociated arms into new forming patches. Note, however, that even at the maxima of the $\langle N_p \rangle$ and $\langle S_p \rangle$ curves, the majority of arms for $\alpha = 0.3$ are still free, as can be corroborated in the upper panel of Figure 9.

DOI: 10.1021/acs.jpcb.7b12229
J. Phys. Chem. B 2018, 122, 4149−4158

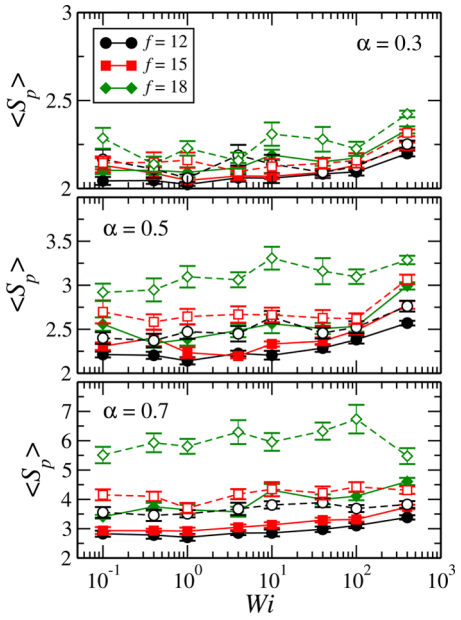

Figure 8. Average number of arms participating in patch formation as a function of the Weissenberg number for SBCs of different functionality (N_{pol} = 40) at λ = 1.0 (filled symbols and continuous lines) and λ = 1.1 (empty symbols and dashed lines).

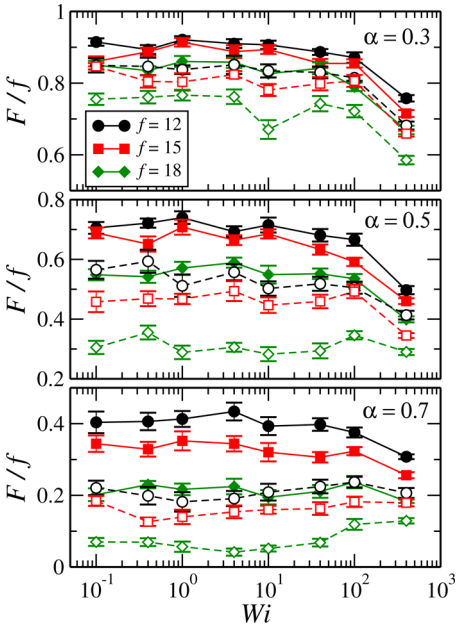

Figure 9. Typical fraction of free arms as a function of the Weissenberg number for SBCs of different functionality (N_{pol} = 40) at λ = 1.0 (filled symbols and continuous lines) and λ = 1.1 (empty symbols and dashed lines).

Accordingly, it is expected that in a concentrated, sheared solution such SBCs will be able to form a variety of different intermolecular transient bonds involving rather weak ones between individual arms and much stronger ones between multiarm patches.

The above scenario maintains its validity in part also for α = 0.5. As can be seen in the middle panel of Figure 6, also in this case, the curves display a increasing trend, expressing the creation of new patches as the shear rate grows. At the same time, however, for f = 15 and f = 18 and for the strongest attraction, λ = 1.1, the expected number of patches $\langle N_p \rangle$ is remarkably insensitive to the shear rate at the values $\langle N_p \rangle \cong 3$ for f = 15 and $\langle N_p \rangle \cong 4$ for f = 18, respectively. The corresponding distribution $P(N_p)$, shown in the middle panel of Figure 5, is also remarkably robust, whereas $\langle S_p \rangle$ shows a moderate growth with Wi, see the middle panel of Figure 8. In both these cases, there exist free arms at equilibrium, but they are in the minority: $F \cong 6$ for f = 15 and $F \cong 5$ for f = 18 (see Figure 9). Accordingly, the SBC at equilibrium consists of a small number of well-organized multiarm patches and a few remaining free chains. The imposed shear has the effect of driving additional free chains onto the existing patches. In this way, the population of the patches is increased without a change in the number of patches themselves.

In this parameter domain, in which $F \lesssim f/2$ but there are still a considerable number of free chains, the SBCs act as robust patchy particles as far as the number of patches is concerned. However, the geometric arrangement of these patches with respect to one another is dramatically influenced by the imposed shear. To quantify this arrangement, we calculate the position of the center of mass for each patch and draw the vectors connecting the star core with those points. Subsequently, we measure the probability distribution function $P(\cos\theta)$ for the mutual angle θ between any pair of those vectors. The results are shown in Figure 10 for the histograms

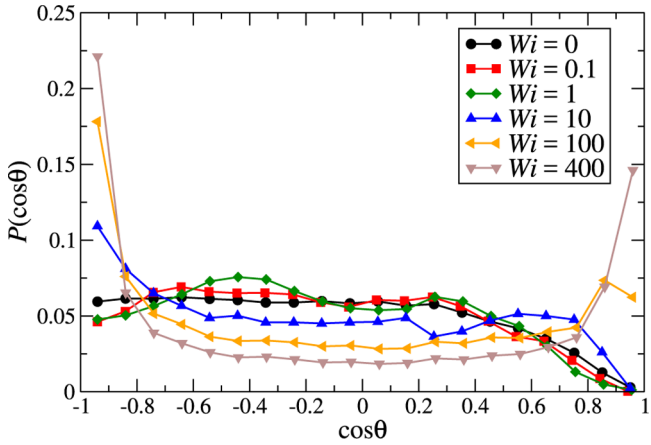

Figure 10. Distribution of the cosine of the angle θ between the vectors connecting the SBC center with the centers of mass of the patches for the case f = 18, α = 0.5, and λ = 1.1 for different values of the Weissenberg number, as indicated in the legend.

and visualized via characteristic simulation snapshots in Figure 11. The number of patches fluctuates around the average value $\langle N_p \rangle$ = 4 for all the values of Wi, but the geometric arrangement of the patches changes markedly. At equilibrium, Wi = 0, the distribution of angles in Figure 10 is rather broad due to the rather short length of the arms, cf. with the well-defined tetrahedral distribution for the much longer arms of the SBCs seen in the previous work at equilibrium.[7] Increasing the shear rate causes a gradual squeezing of the star toward the flow-vorticity plane and the patches assume a concomitant planar configuration with two of them pointing "forward" and two of them "backward", see Figure 11 panels (c) and (g). At the highest value shown, Wi = 400, there are two pairs of patches on either side, bringing forward a bimodal distribution $P(\cos\theta)$ with two pronounced maxima at $\cos\theta = \pm 1$. At the

DOI: 10.1021/acs.jpcb.7b12229
J. Phys. Chem. B 2018, 122, 4149−4158

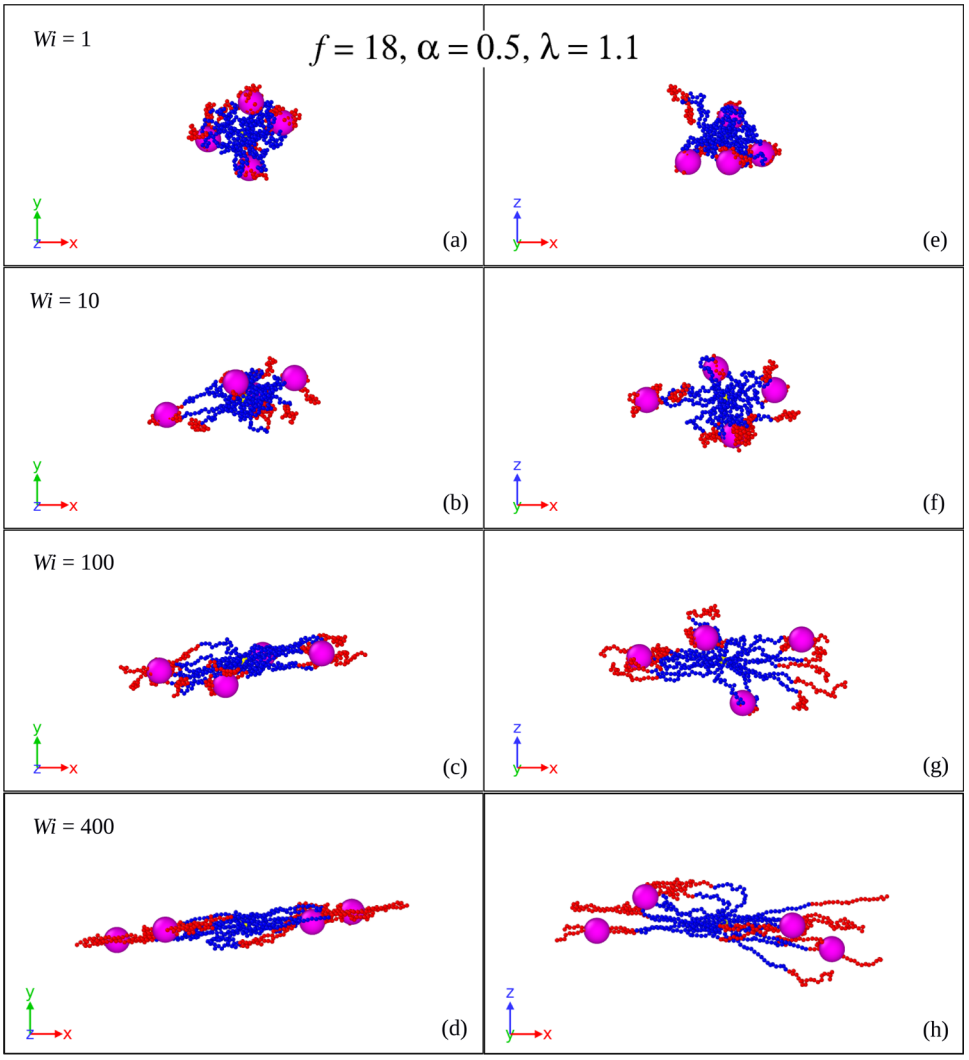

Figure 11. Characteristic simulation snapshots[30] of the SCB (f = 18, α = 0.5, λ = 1.1) under shear at increasing Weissenberg numbers as indicated on the panels. The left column displays the conformations on the flow-gradient plane, seen from the vorticity axis, whereas the right column shows the conformations on the flow-vorticity plane, seen from the gradient axis. Solvophilic and solvophobic monomers are rendered as blue and red beads, respectively. The larger magenta spheres are centered at the centers of mass of the patches built by the end groups.

same time, a few arms break free and rotate on the flow-vorticity plane, see Figure 11, panel (h).

A third pattern of behavior of SBCs under shear is finally observed for the highest fraction of attractive monomers, α = 0.7 seen at the bottom panels of Figures 6 and 8. One encounters the already discussed scenario of $\langle N_p \rangle$ remaining unaffected by shear but, in addition to it, for the cases f = 18, λ = 1.0 and f = 18, λ = 1.1, a new scenario shows up. Here, the average number of patches $\langle N_p \rangle$ first decreases with increasing Wi accompanied by a simultaneous increase in $\langle S_p \rangle$, see the empty and filled diamonds in Figures 6 and 8. At very high shear rates, the trend reverses itself: the number of patches increases and their population becomes smaller. It can be easily seen that this is happening for the cases in which there are hardly any free arms for the SBC at equilibrium, as shown in the bottom panel of Figure 9. All of the linear chains are organized in patches of 3 or 4 members and the attractions are too strong for the patches to be destroyed under moderate or even high shear. Accordingly, the effect of the external drive is to drive the fusion of existing, big patches into new, bigger ones, thus decreasing their number and increasing their population. However, these patches are now too bulky, so that at very high shear rates, the shear is capable of breaking them up. It is now fission of big patches that reverses the trend and makes $\langle N_p \rangle$ go up and $\langle S_p \rangle$ go down. In all the cases, the number of free arms is very low and $F \ll f$ holds. As already mentioned, the whole patch rearrangement scenario is accompanied by interesting dynamical aspects such as tumbling and arm rotation. These topics deserve a careful analysis on their own and would be presented in a detailed way in the future, specially in the light of a very recent study suggesting the need to separate different relaxation (rotation, oscillation, and breathing) modes to describe the dynamics of athermal star polymers under shear.[32,33]

CONCLUSIONS

The behavior of patchiness and shape of low-functionality, star block-copolymers in shear flow have been quantitatively analyzed for different values of amphiphilicity and solvent quality. This has been achieved for Weissenberg numbers ranging from Wi = 0 (equilibrium) to larger than 10^3, the latter lying deeply into the nonlinear regime. We have shown that

DOI: 10.1021/acs.jpcb.7b12229
J. Phys. Chem. B 2018, 122, 4149−4158

these polymers respond to shear stresses qualitatively differently from athermal stars when the attraction between their solvophobic blocks is sufficiently high and that shear can be utilized as yet another parameter in tuning their self-assembly next to functionality, amphiphilicity, solvent quality, and temperature. Although shear increases the patchiness of low-amphiphilicity SBCs as a result of their alignment with the flow field, we have found that for high-amphiphilicity stars, the number and size of patches formed are nonmonotonic functions of shear rate. This might have interesting implications on the system's rheological properties and viscoelastic responses in dilute bulk phases because the macro- and microscopic phase behaviors of SBCs in equilibrium are governed by their number of association sites, or patches. Furthermore, we were able to demonstrate that high-amphiphilicity SBCs deform differently than athermal star polymers in the regime of intermediate Weissenberg numbers.

The understanding of how the average number of patches $\langle N_p \rangle$ changes depending on the system parameters (f, N_{pol}, α, λ, Wi) is a key point to tune the functionalization of these molecular building blocks, and hence their hierarchical self-assembling process, without the need to change the molecules in solution.[7] We have found quasiuniversal characteristics of the shape and patchiness of the SBCs under flow, which show that knowledge of the star properties in equilibrium can lead to reliable predictions for its behavior in different regimes of the shear rate. In particular, the key factors in determining the evolution of the star patchiness and shape under shear are (i) the presence (or absence) of any nonassociated arms at equilibrium and (ii) the spatial extent of the original patches. The main mechanisms for patch evolution under shear have been established, these being (i) merging of free arms into new patches, (ii) fusion of two patches into one, and (iii) fission of existing, bulky patches under strong shear. The antagonistic effects of these sometimes bring about nonmonotonic effects on the dependence of patchiness under shear. The influence of these patch rearrangements on the rheology of concentrated systems and the investigation on whether the characteristics of single-star polymers found in this study will prevail in the systems of finite densities will be the subject of further theoretical and computational studies in the future.

AUTHOR INFORMATION

Corresponding Authors

*E-mail: christos.likos@univie.ac.at (C.N.L.).
*E-mail: manuel.camargo@uan.edu.co (M.C.).

ORCID

Christos N. Likos: 0000-0003-3550-4834
Manuel Camargo: 0000-0003-0276-2650

Present Address

§Centro de Física de Materiales (CSIC, UPV/EHU), Paseo Manuel de Lardizabal 5, E-20018 San Sebastian, Spain (M.F.).

Notes

The authors declare no competing financial interest.

ACKNOWLEDGMENTS

The authors thank support by the European Training Network COLLDENSE (H2020-MCSA-ITN-2014, Grant No. 642774). This publication is based upon work partially supported by the King Abdullah University of Science and Technology (KAUST) Office of Sponsored Research (OSR) under Award No. OSR-2016-CRG5-3073. M.C. thanks VCTI-UAN (Project 2015036) and Colciencias (Project 123365842816). Computer time at the Vienna Scientific Cluster (VSC) is gratefully acknowledged.

REFERENCES

(1) Ripoll, M.; Winkler, R. G.; Gompper, G. Star polymers in shear flow. *Phys. Rev. Lett.* **2006**, *96*, No. 188302.
(2) Bianchi, E.; Blaak, R.; Likos, C. N. Patchy colloids: state of the art and perspectives. *Phys. Chem. Chem. Phys.* **2011**, *13*, 6397−6410.
(3) Wang, Y.; Wang, Y.; Breed, D. R.; Manoharan, V. N.; Feng, L.; Hollingsworth, A. D.; Weck, M.; Pine, D. J. Colloids with valence and specific directional bonding. *Nature* **2012**, *491*, 51−55.
(4) Chen, Q.; Bae, S. C.; Granick, S. Directed self-assembly of a colloidal kagome lattice. *Nature* **2011**, *469*, 381−384.
(5) Choueiri, R. M.; Galati, E.; Thérien-Aubin, H.; Klinkova, A.; Larin, E. M.; Querejeta-Fernández, A.; Han, L.; Xin, H. L.; Gang, O.; Zhulina, E. B.; et al. Surface patterning of nanoparticles with polymer patches. *Nature* **2016**, *538*, 79−83.
(6) Capone, B.; Coluzza, I.; Lo Verso, F.; Likos, C. N.; Blaak, R. Telechelic star polymers as self-assembling units from the molecular to the macroscopic scale. *Phys. Rev. Lett.* **2012**, *109*, No. 238301.
(7) Rovigatti, L.; Capone, B.; Likos, C. N. Soft self-assembled nanoparticles with temperature-dependent properties. *Nanoscale* **2016**, *8*, 3288−3295.
(8) Gârlea, I. C.; Bianchi, E.; Capone, B.; Rovigatti, L.; Likos, C. N. Hierarchical self-organization of soft patchy nanoparticles into morphologically diverse aggregates. *Curr. Opin. Colloid Interface Sci.* **2017**, *30*, 1−7.
(9) Lo Verso, F.; Likos, C. N.; Löwen, H. Computer simulation of thermally sensitive telechelic star polymers. *J. Phys. Chem. C* **2007**, *111*, 15803−15810.
(10) Capone, B.; Coluzza, I.; Blaak, R.; Lo Verso, F.; Likos, C. N. Hierarchical self-assembly of telechelic star polymers: from soft patchy particles to gels and diamond crystal. *New J. Phys.* **2013**, *15*, No. 095002.
(11) Koch, C.; Panagiotopoulos, A. Z.; Lo Verso, F.; Likos, C. N. Customizing wormlike mesoscale structures via self-assembly of amphiphilic star polymers. *Soft Matter* **2015**, *11*, 3530−3535.
(12) Wadgaonkar, I.; Chatterji, A. Network formation and gelation in telechelic star polymers. *J. Chem. Phys.* **2017**, *146*, No. 084906.
(13) Winkler, R. G.; Fedosov, D. A.; Gompper, G. Dynamical and rheological properties of soft colloid suspensions. *Curr. Opin. Colloid Interface Sci.* **2014**, *19*, 594−610.
(14) Vlassopoulos, D.; Cloitre, M. Tunable rheology of dense soft deformable colloid. *Curr. Opin. Colloid Interface Sci.* **2014**, *19*, 561−574.
(15) Saha Dalal, I.; Albaugh, A.; Hoda, N.; Larson, R. G. Tumbling and deformation of isolated polymer chains in shearing flow. *Macromolecules* **2012**, *45*, 9493−9499.
(16) Dalal, I. S.; Hoda, N.; Larson, R. G. Multiple regimes of deformation in shearing flow of isolated polymers. *J. Rheol.* **2012**, *56*, 305−332.
(17) Chen, W.; Chen, J.; Liu, L.; Xu, X.; An, L. Effects of chain stiffness on conformational and dynamical properties of individual ring polymers in shear flow. *Macromolecules* **2013**, *46*, 7542−7549.
(18) Chen, W.; Li, Y.; Zhao, H.; Liu, L.; Chen, J.; An, L. Conformations and dynamics of single flexible ring polymers in simple shear flow. *Polymer* **2015**, *64*, 93−99.
(19) Ripoll, M.; Winkler, R. G.; Gompper, G. Hydrodynamic screening of star polymers in shear flow. *Eur. Phys. J. E* **2007**, *23*, 349−354.
(20) Yamamoto, T.; Masaoka, N. Numerical simulation of star polymers under shear flow using a coupling method of multi-particle collision dynamics and molecular dynamics. *Rheol. Acta* **2015**, *54*, 139−147.
(21) Nikoubashman, A.; Likos, C. N. Branched polymers under shear. *Macromolecules* **2010**, *43*, 1610−1620.

DOI: 10.1021/acs.jpcb.7b12229
J. Phys. Chem. B 2018, 122, 4149−4158

(22) Myung, J. S.; Taslimi, F.; Winkler, R. G.; Gompper, G. Self-organized structures of attractive end-functionalized semiflexible polymer suspensions. *Macromolecules* **2014**, *47*, 4118−4125.
(23) Taslimi, F.; Gompper, G.; Winkler, R. G. Scaffold structures by telechelic rodlike polymers: Nonequilibrium structural and rheological properties under shear flow. *Macromolecules* **2014**, *47*, 6946−6954.
(24) Malevanets, A.; Kapral, R. Mesoscopic model for solvent dynamics. *J. Chem. Phys.* **1999**, *110*, 8605−8613.
(25) Malevanets, A.; Kapral, R. Solute molecular dynamics in a mesoscale solvent. *J. Chem. Phys.* **2000**, *112*, 7260−7269.
(26) Frenkel, D.; Smit, B. *Understanding Molecular Simulation: From Algorithms to Applications*; Academic Press, 2001.
(27) Huang, C. C.; Chatterji, A.; Sutmann, G.; Gompper, G.; Winkler, R. G. Cell-level canonical sampling by velocity scaling for multiparticle collision dynamics simulations. *J. Comput. Phys.* **2010**, *229*, 168−177.
(28) Doi, M.; Edwards, S. F. *The Theory of Polymer Dynamics*; Oxford University Press, 1986.
(29) Egorov, S. A.; Paturej, J.; Likos, C. N.; Milchev, A. Controlling the interactions between soft colloids via surface adsorption. *Macromolecules* **2013**, *46*, 3648−3653.
(30) Stukowski, A. Visualization and analysis of atomistic simulation data with OVITO - the Open Visualization Tool. *Modell. Simul. Mater. Sci. Eng.* **2010**, *18*, No. 015012.
(31) Grest, G. S.; Kremer, K.; Witten, T. A. Structure of many arm star polymers: a molecular dynamics simulation. *Macromolecules* **1987**, *20*, 1376−1383.
(32) Sablić, J.; Praprotnik, M.; Delgado-Buscalioni, R. Deciphering the dynamics of star molecules in shear flow. *Soft Matter* **2017**, *13*, 4971−4987.
(33) Sablić, J.; Delgado-Buscalioni, R.; Praprotnik, M. Application of the Eckart frame to soft matter: rotation of star polymers under shear flow. *Soft Matter* **2017**, *13*, 6988−7000.

DOI: 10.1021/acs.jpcb.7b12229
J. Phys. Chem. B 2018, 122, 4149−4158